

p38 and OGT Sequestration into Viral Inclusion Bodies in Cells Infected with Human Respiratory Syncytial Virus Suppresses MK2 Activities and Stress Granule Assembly

Jens Fricke,^a Lily Y. Koo,^b Charles R. Brown,^{c*} Peter L. Collins^a

Laboratory of Infectious Diseases,^a Research and Technology Branch,^b and Laboratory of Molecular Microbiology,^c National Institute of Allergy and Infectious Diseases, National Institutes of Health, Bethesda, Maryland, USA

Respiratory syncytial virus (RSV) forms cytoplasmic inclusion bodies (IBs) that are thought to be sites of nucleocapsid accumulation and viral RNA synthesis. The present study found that IBs also were the sites of major sequestration of two proteins involved in cellular signaling pathways. These are phosphorylated p38 mitogen-activated protein kinase (MAPK) (p38-P), a key regulator of cellular inflammatory and stress responses, and O-linked *N*-acetylglucosamine (OGN) transferase (OGT), an enzyme that catalyzes the posttranslational addition of OGN to protein targets to regulate cellular processes, including signal transduction, transcription, translation, and the stress response. The virus-induced sequestration of p38-P in IBs resulted in a substantial reduction in the accumulation of a downstream signaling substrate, MAPK-activated protein kinase 2 (MK2). Sequestration of OGT in IBs was associated with suppression of stress granule (SG) formation. Thus, while the RSV IBs are thought to play an essential role in viral replication, the present results show that they also play a role in suppressing the cellular response to viral infection. The sequestration of p38-P and OGT in IBs appeared to be reversible: oxidative stress resulting from arsenite treatment transformed large IBs into a scattering of smaller bodies, suggestive of partial disassembly, and this was associated with MK2 phosphorylation and OGN addition. Unexpectedly, the RSV M2-1 protein was found to localize in SGs that formed during oxidative stress. This protein was previously shown to be a viral transcription elongation factor, and the present findings provide the first evidence of possible involvement in SG activities during RSV infection.

Human respiratory syncytial virus (RSV) is the most important viral agent of severe respiratory tract disease in infants and young children worldwide. RSV is a cytoplasmic, enveloped virus with a nonsegmented negative-strand RNA genome that is classified in the genus *Pneumovirus*, family *Paramyxoviridae* (1). There presently is no specific anti-RSV therapy or vaccine, although infants at high risk for severe RSV disease due to underlying conditions can be substantially protected by passive antibody immunoprophylaxis (2).

RSV forms cytoplasmic inclusion bodies (IBs) during infection, as also has been reported for measles virus and human metapneumovirus, also of the family *Paramyxoviridae* (3–5). In the case of RSV, the IBs have been shown to contain the RSV nucleoprotein (N), phosphoprotein (P), M2-1 protein, and large polymerase (L) protein (4, 6). The expression of viral N and P proteins is sufficient for the appearance of IBs (4, 7). Viral genomic RNA also localizes in IBs (8), consistent with the presumption that these are sites of nucleocapsid assembly and RNA synthesis. Furthermore, heat shock protein Hsp70 has been shown to associate with IBs, although no functional role was determined (9). Overall, the formation and function of the IBs are not well understood.

As an obligate intracellular parasite, RSV interacts with host signaling networks and machinery both to block antiviral responses and to promote viral replication. Previous work implicated the mitogen-activated protein kinases (MAPKs), in particular the extracellular signal-regulated kinase (ERK) and p38 MAPK, in the tropism as well as entry of RSV (10–12). The p38 MAPK is a central mediator involved in regulating cellular inflammatory and stress responses, as well as cellular protein synthesis (13, 14). Thus, any alteration of p38 signaling during a viral infection has the potential for multifold impact on virus-host interactions.

p38 and one of its downstream substrates, MAPK-activated protein kinase 2 (MK2), play important roles in posttranscriptional mRNA metabolism during stress conditions. In particular, activated MK2 promotes the stability of AU-rich element (ARE)-containing mRNAs, such as those encoding proinflammatory and antiviral proteins, including beta interferon (IFN- β), interleukin 1 β (IL-1 β), and tumor necrosis factor alpha (TNF- α) (15–17). Thus, interference with signal transduction through p38 and MK2 can reduce the stability of the mRNAs encoding these innate response proteins and thereby reduce their production.

Of the four p38 isoforms (α , β , γ , and δ), p38 α appears to be responsible for MK2 activation. Thermodynamic and steady-state kinetic characterization using p38 α indicated a high-affinity binding with MK2 (K_d [equilibrium dissociation constant] = 2.5 nM), and the complex is required in stress dependent-activation of MK2 (18, 19). Furthermore, the formation of this complex seems to be critical for the stabilization of both proteins, as p38 accumulation is significantly reduced in MK2-deficient cells and, con-

Received 22 August 2012 Accepted 2 November 2012

Published ahead of print 14 November 2012

Address correspondence to Jens Fricke, frickej@niaid.nih.gov.

* Present address: Charles R. Brown, Translational Science, MedImmune, Gaithersburg, Maryland, USA.

Supplemental material for this article may be found at <http://dx.doi.org/10.1128/JVI.02263-12>.

Copyright © 2013, American Society for Microbiology. All Rights Reserved.

doi:10.1128/JVI.02263-12

The authors have paid a fee to allow immediate free access to this article.

versely, MK2 accumulation is reduced in p38 α -knockout mouse embryonic fibroblasts (20, 21). Earlier studies could not rule out a role for the β isoform because the inhibitors involved affected both p38 α and p38 β (22), but subsequent studies showed that MK2 stability and signaling are unaffected in knockout mice lacking the p38 β isoform (23).

Another aspect of the cellular response to stress is the formation of stress granules (SGs). These are complex ribonucleoprotein aggregates that contain untranslated mRNAs and form under stress conditions. SGs constitute an important intermediate step in the equilibrium between active translation and mRNA decay (24). Regulation of SG dynamics involves posttranslational modifications of a number of proteins by methylation, acetylation, phosphorylation, and the addition of O-linked *N*-acetylglucosamine (OGN). In particular, OGN-modification, mediated by OGN-transferase (OGT), of various ribosomal proteins is required for the aggregation of untranslated messenger ribonucleoproteins and assembly into SGs (25–27). Interestingly, p38 has been shown to interact with and recruit OGT to specific targets (28, 29).

Numerous viruses have been shown to manipulate or modulate SG pathways to impact translation and potentially affect innate antiviral mechanisms (27). The role of SGs in RSV infection remains to be elucidated. In one study, SGs were thought to promote RSV replication (8). Meanwhile, a separate study suggested that RSV subverts SG formation (30). In the present study, we showed that RSV sequesters phosphorylated p38 (p38-P) and OGT into viral IBs. This has the effect of suppressing the MK2 pathway and SG assembly during RSV infection.

MATERIALS AND METHODS

Cells. A549 cells (ATCC CCL-185) were grown in F-12K medium (ATCC) containing 10% fetal bovine serum (FBS). Vero cells were grown in Opti-MEM 1 medium (Invitrogen) containing 10% FBS. The respective media containing 2% FBS were used during all experiments described below.

Virus, infection, and inhibitor. Recombinant RSV (rA2) was constructed from the wild-type A2 strain as previously described (31). Virus stocks were propagated and titrated on Vero cells. For titration, plaques were stained using monoclonal antibodies (MAbs) specific to RSV F protein, followed by peroxidase-labeled anti-mouse IgG(H+L) (KPL) for detection. RSV was added to A549 cells at a multiplicity of infection (MOI) of 0.5 PFU per cell for all experiments unless indicated otherwise. Inhibitor CMPD-1 [4-(2'-fluorobiphenyl-4-yl)-*N*-(4-hydroxyphenyl)-butyramide] (EMD Biosciences or Tocris), which selectively inhibits the phosphorylation of MK2 by p38 α , was prepared as a stock solution in dimethyl sulfoxide (DMSO) and used at a final concentration of 50 μ M (32). Mock-treated cells were given an equivalent amount of DMSO (final concentration, 0.2%).

RSV-specific FISH. Fluorescence *in situ* hybridization (FISH) was performed as previously described (33) and adapted for the present study. Briefly, cells were fixed with 4% paraformaldehyde cells and hybridized overnight at 50°C with a mixture of antisense digoxigenin-UTP-labeled riboprobes representing the RSV N, P, M2-1, NS1, NS2, and F genes. These probes were 285 to 432 nucleotides in length (sequences are available upon request) and were synthesized commercially (Lofstrand Labs, Ltd., Gaithersburg, MD). Following hybridization, cells were blocked with 2% horse serum, 2% sheep serum, and 0.2% fish skin gelatin in 0.1 M Tris (pH 7.4) buffer and incubated with sheep anti-digoxigenin-alkaline phosphatase (Roche Molecular Biochemicals). Finally, for detection and visualization, Alexa 594-conjugated tyramide (Invitrogen) was applied in a tyramide signal amplification diluent (1:100) (PerkinElmer). Samples were then rinsed sequentially in 0.1 M Tris (pH 7.4) containing 0.1%

Tween 20, 0.1 M Tris (pH 7.4), and phosphate-buffered saline (PBS) and were mounted in ProLong Gold antifade reagent containing the nuclear stain 4',6-diamidino-2-phenylindole (DAPI) (Invitrogen). Samples were analyzed by confocal microscopy.

Confocal microscopy. Fluorescent images were captured on a Leica TCS-SP5 confocal microscope (Leica Microsystems, Germany) equipped with a white light laser using a 63 \times /NA1.4 oil immersion objective. The dynamic range of pixel intensities was determined so to avoid saturation of the brightest signal (such as in the dense IB aggregates) in an experiment. Each image was taken as a z-stack of 0.25- μ m-thick slices. Except as noted, each final image is presented as a maximum projection of the stacked images, in which a two-dimensional image is created using the brightest pixel values in the z-series. In some cases, as noted, individual slices from a z-stack of images are shown. In some cases, as noted, 3-dimensional renderings were constructed from a z-stack of images to illustrate colocalizations. Huygens Essential (version 3.6; Scientific Volume Imaging, the Netherlands), Leica Lite (version 2.6.0; Leica Microsystems, Germany), and Imaris (version 7.1; Bitplane AG, Switzerland) were used for deconvolution and image processing.

Antibodies. Polyclonal antibodies (PAb) against p38 α , MAb against p38-P, MAb against M2-1, PAb against OGT, and PAb against β -actin were obtained from Abcam. MAb against P was obtained from Antibodies-Online. MAb against OGN was obtained from Covance. MAb against MK2 was obtained from Epitomics. PAb against TIA-1 was obtained from Santa Cruz Biotechnology. MAb against eukaryotic initiation factor 3 (eIF3) was obtained from Cell Signaling. Two different preparations of PAb against RSV were used: for Western blotting, we used a rabbit PAb that we prepared using sucrose gradient-purified RSV that had been denatured and reduced, and for immunofluorescence, we used a goat PAb that was obtained from AbD Serotec. Secondary antibodies used for Western blotting were species specific, affinity purified, and peroxidase labeled (KPL). Secondary species-specific antibodies used for immunofluorescence were labeled with either Alexa 488 (Invitrogen or Jackson ImmunoResearch) or Alexa 594 or Alexa 647 (Invitrogen).

Immunofluorescence. Cells were fixed in 4% paraformaldehyde in Hanks' balanced salt solution for 15 min at room temperature and were permeabilized with 1% Triton X-100 (Roche) in PBS for 5 min. The cells were subsequently stained with primary and appropriate fluorescent dye-labeled secondary antibodies and analyzed by confocal microscopy as described above.

Western blot analysis. Cells were lysed in NuPAGE LDS sample buffer (Invitrogen) supplemented with 1 \times phosphatase (PhosSTOP; Roche) and 1 \times protease inhibitor (Complete, Roche). The lysate was centrifuged through a QIAshredder Mini Spin Column (Qiagen) and subjected to heat denaturation with 2-mercaptoethanol (Sigma). Equal amounts of cell lysate were separated using 4 to 12% Novex Tris glycine gels (Invitrogen) and transferred to polyvinylidene difluoride (PVDF) membranes using an iBlot gel transfer device (Invitrogen). The membrane was incubated with primary and peroxidase-conjugated secondary antibodies. Specific bands were visualized by chemiluminescence using SuperSignal West Pico substrate (Thermo Scientific) and exposure to BioMax LIGHT films (Kodak).

RESULTS

Effects of RSV infection on p38-P distribution. To investigate the role of the p38/MK2 pathway in RSV infection, we treated human airway epithelial A549 cells with inhibitor CMPD-1, which selectively inhibits p38/MK2 signaling by inhibiting phosphorylated p38 α from phosphorylating and activating MK2 (32). Treatment with inhibitor CMPD-1 was initiated 30 min before infection to assess any inhibitory effect on viral entry or 75 min after infection, following virus adsorption. Viral infection was assessed 18 h postinfection by Western blotting using a rabbit antiserum raised against sucrose gradient-purified RSV, PAb specific to p38 α , and a MAb specific to p38-P (Fig. 1). This showed that the level of p38 α

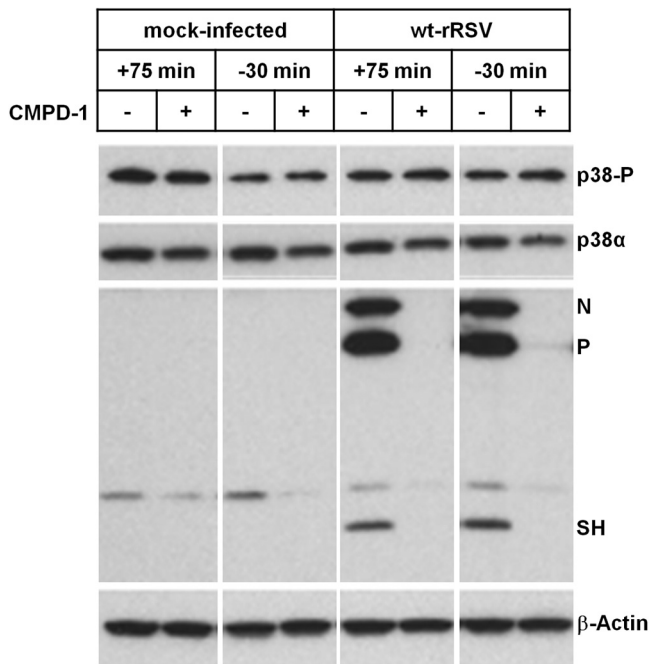


FIG 1 Western blot analysis of the intracellular expression of p38α, p38-P, and RSV proteins in response to RSV infection and treatment with inhibitor CMPD-1. Monolayer cultures of A549 cells were infected with recombinant wild-type RSV (wt-rRSV) at an MOI of 0.5 or were mock infected. Replicate cultures were treated with the inhibitor CMPD-1 or mock treated, beginning 30 min before infection (−30 min) or 75 min postinfection (+75 min). The cultures were harvested 18 h postinfection and analyzed by Western blotting with antibodies against p38α, p38-P, and purified RSV (which reacted here with the N, P, and SH proteins) and β-actin as a loading control. The antibodies to p38α and p38-P did not cross-react, and different exposure times were used (1 min for p38α, 10 min for p38-P, 20 s for RSV, and 3 s for actin), and thus these results do not indicate the relative abundance of p38α versus p38-P.

was not affected by treatment with this inhibitor. The level of p38-P also was unchanged by treatment with inhibitor CMPD-1 beginning at either time and was relatively unchanged by RSV infection compared to mock infection.

In contrast, treatment with the inhibitor beginning at either time significantly inhibited viral protein synthesis (Fig. 1). Since inhibition was effective regardless of the time of administration, the inhibitor presumably did not interfere with viral entry but, rather, acted at a step further downstream. Further investigation showed that the overall synthesis of cellular proteins also was substantially inhibited by the inhibitor treatment (data not shown). This suggested that there was constitutive signaling through the p38-P/MK2 pathway and that this was necessary for ongoing protein synthesis in RSV-infected and mock-infected cells.

Consistent with the strong inhibition of viral protein synthesis observed in Fig. 1, only trace amounts of infectious virus were recovered from RSV-infected cells treated with inhibitor CMPD-1 (Fig. 2A). Furthermore, *in situ* hybridization of RSV-infected cells with a fluorescent dye-labeled viral RNA probe revealed only a small amount of viral RNA present in cells incubated in the presence of inhibitor CMPD-1, and this small level of RNA might have come from the input inoculum. In contrast, in the absence of inhibitor, viral RNA was readily detected in cytoplasmic aggregates (Fig. 2B) that were subsequently identified as viral IBs by the

presence of viral P and M2-1 proteins detected by immunofluorescence (Fig. 3 and 4). The presence of RSV RNA in IBs had been documented previously (8). The accumulation of viral RNA in the IBs was maximal at 18 h postinfection, and the formation of IBs was most developed in terms of size at this time; therefore, 18 h postinfection was chosen for all subsequent experiments.

We also investigated whether RSV infection altered the cellular localization of p38-P. A549 cells were mock infected or infected with RSV, were treated or not with inhibitor CMPD-1 beginning 30 min before infection or 75 min postinfection, and at 18 h postinfection were analyzed by immunofluorescence staining with an antibody specific to p38-P. The results revealed striking differences in cellular localization of p38-P under the various conditions (Fig. 3: the results shown are with the inhibitor added 75 min postinfection; the results with the inhibitor added 30 min before infection were indistinguishable and are not shown). In mock-infected cells, p38-P was detected as a diffuse signal throughout the cytoplasm (Fig. 3 and 4; the diffuse pattern is barely visible because the signal intensities of all of the images were reduced equally to avoid saturation of the more intense signals). In contrast, in RSV-infected cells, p38-P was found in dense cytoplasmic aggregates (Fig. 3 and 4). The appearance of this dense staining was not due to an increase in synthesis or stability, as was shown by the Western blot in Fig. 1. These aggregates were identified as viral IBs based on costaining with MAbs against the viral M2-1 (Fig. 3 and 4A) and P (Fig. 4B) proteins, as well as by the presence of RSV RNA as already shown (Fig. 2B) (8). Infected cells treated with inhibitor CMPD-1 either 30 min before or 75 min after infection failed to form viral IBs, as would be expected since viral protein synthesis was strongly inhibited. These cells lacked detectable aggregation of p38-P (Fig. 3). The colocalization of p38-P with the viral M2-1 and P proteins was further illustrated by cross-sectional analysis and intensity profiling (Fig. 4). This showed that p38-P, M2-1, and P accumulated throughout the IBs, although the viral proteins tended to concentrate more heavily toward the periphery of the large IBs.

Effects of RSV infection on MK2 accumulation. Since RSV infection did not appear to affect the accumulation and phosphorylation of p38 but drastically changed its intracellular localization, we examined the accumulation and phosphorylation status of its downstream signaling substrate MK2. Following the same treatment and infection protocol as in the previous experiments, cell lysates were prepared 18 h postinfection and analyzed by Western blotting with a MAb against MK2/MK2-P. This showed that phosphorylation of MK2 in mock-infected cells was below the limit of detection under these conditions (Fig. 5A). The results also showed that treatment of mock-infected cells with inhibitor CMPD-1 resulted in a substantial decrease in the level of MK2. This reduction in MK2 presumably was due to protein instability as a result of perturbed p38/MK2 binding due to CMPD-1, as well as insufficient MK2 replacement due to the overall inhibition of protein synthesis. Remarkably, infection with RSV also resulted in a strong reduction in the level of MK2 (Fig. 5A) and in this regard mimicked the outcome of the inhibitor. However, in this case, we suggest that the loss of MK2 was a result of the sequestration of p38-P in the IBs, making it unavailable to bind to and stabilize MK2. The addition of inhibitor to RSV-infected cells had no additional effect on the accumulation of MK2. As a positive control for activation of MK2, we subjected mock-infected cells to a 30-min treatment with arsenite, which is known to strongly induce

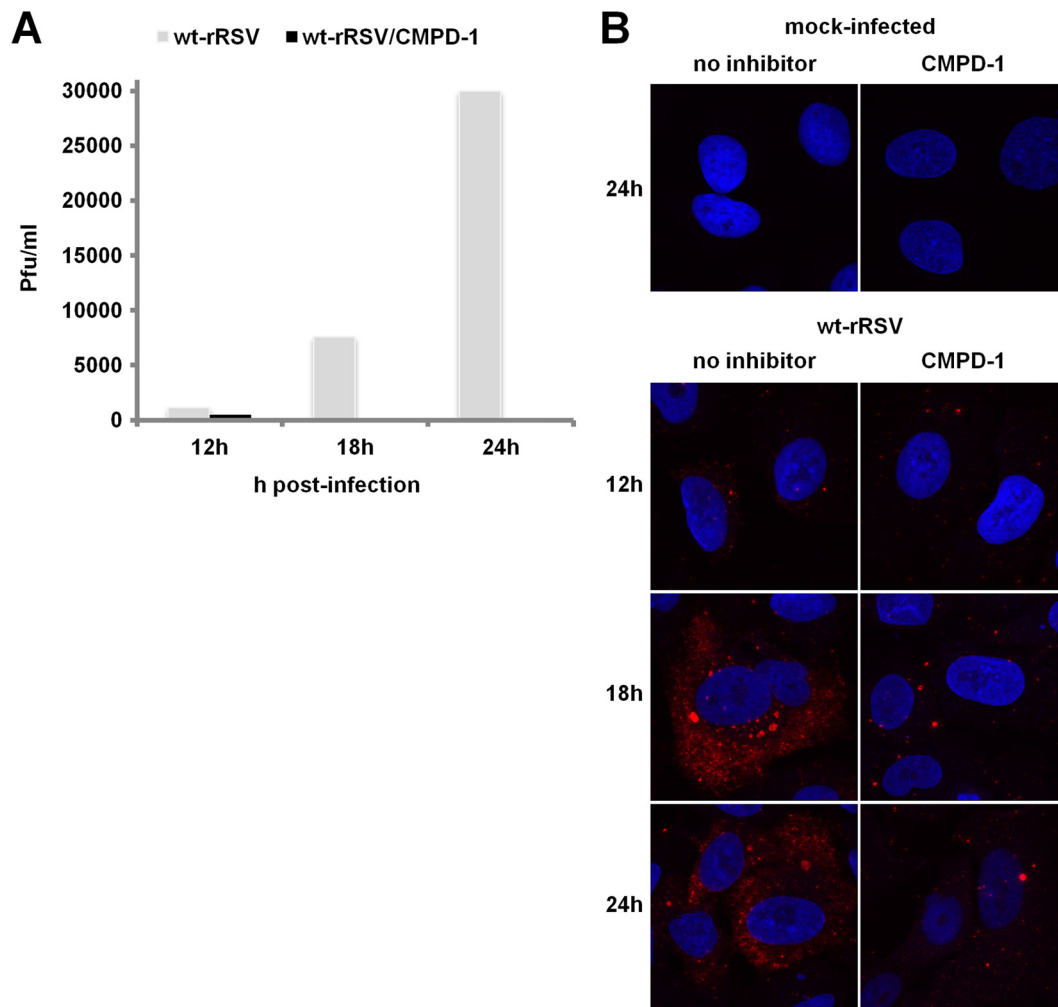


FIG 2 Effect of CMPD-1 treatment on RSV replication and RNA synthesis. Monolayer cultures of A549 cells were infected with wt-rRSV at an MOI of 0.5 or were mock infected. Cultures were treated with the inhibitor CMPD-1 or mock treated beginning 75 min postinfection and were incubated for a total of 18 h. (A) RSV replication. The cell culture medium, from two replicate cultures per time point, was collected at 12 h, 18 h, and 24 h postinfection, and viral titers were determined by plaque assay. (B) FISH images of RSV-infected cells. Cultures were fixed and hybridized with a set of RNA probes specific to the N, P, M2-1, NS1, NS2, and F genes (red), and nuclei were stained with DAPI (blue). The samples were analyzed by confocal microscopy.

oxidative stress. Under these conditions, essentially all of the MK2 was converted to MK2-P (Fig. 5), demonstrating the expected strong activation of the p38/MK2 pathway under stress conditions. When RSV-infected cells were similarly treated with arsenite for 30 min at 18 h postinfection, the MK2 protein, which was present at a greatly reduced level as already noted, was quantitatively converted to its activated, phosphorylated form, MK2-P (Fig. 5B).

The finding that MK2 was phosphorylated in RSV-infected cells following arsenite treatment was somewhat surprising, given that p38-P was sequestered in IBs in untreated RSV-infected cells. We therefore examined the localization of p38-P by immunofluorescence (Fig. 6). Following the brief arsenite treatment, immunostaining of RSV-infected cells with the P-specific (Fig. 6A) or M2-1-specific (Fig. 6B) MAb revealed IBs that appeared to be smaller and more numerous than in RSV-infected cells that were mock treated in parallel. This suggested that the arsenite treatment had the effect of disrupting the IBs. The observed MK2 ac-

tivation in the case of the infected cells could be due, at least in part, to released p38-P.

Effects of RSV infection on OGT distribution and SG formation. As noted above (see the introduction), p38 and MK2 play important roles in posttranscriptional regulation of mRNA metabolism under stress conditions, roles that also involve SGs and OGT. p38 also binds to and recruits OGT (28, 29), which, in turn, mediates OGN modification of key target proteins that is necessary for aggregation of untranslated mRNA-containing ribonucleoproteins into SGs (26). Given the effects of RSV infection on the localization, accumulation, and activation of p38-P and MK2, we used immunofluorescence staining to investigate possible effects on OGT and SGs.

RSV-infected cells were analyzed at 18 h postinfection with antibodies specific to OGT, to the SG marker TIA-1, and to viral P (Fig. 7) or M2-1 protein (Fig. 8). Mock-infected cells exhibited a diffuse distribution of OGT (Fig. 7A and 8A; the diffuse pattern is barely visible because the signal intensities of all of the images were

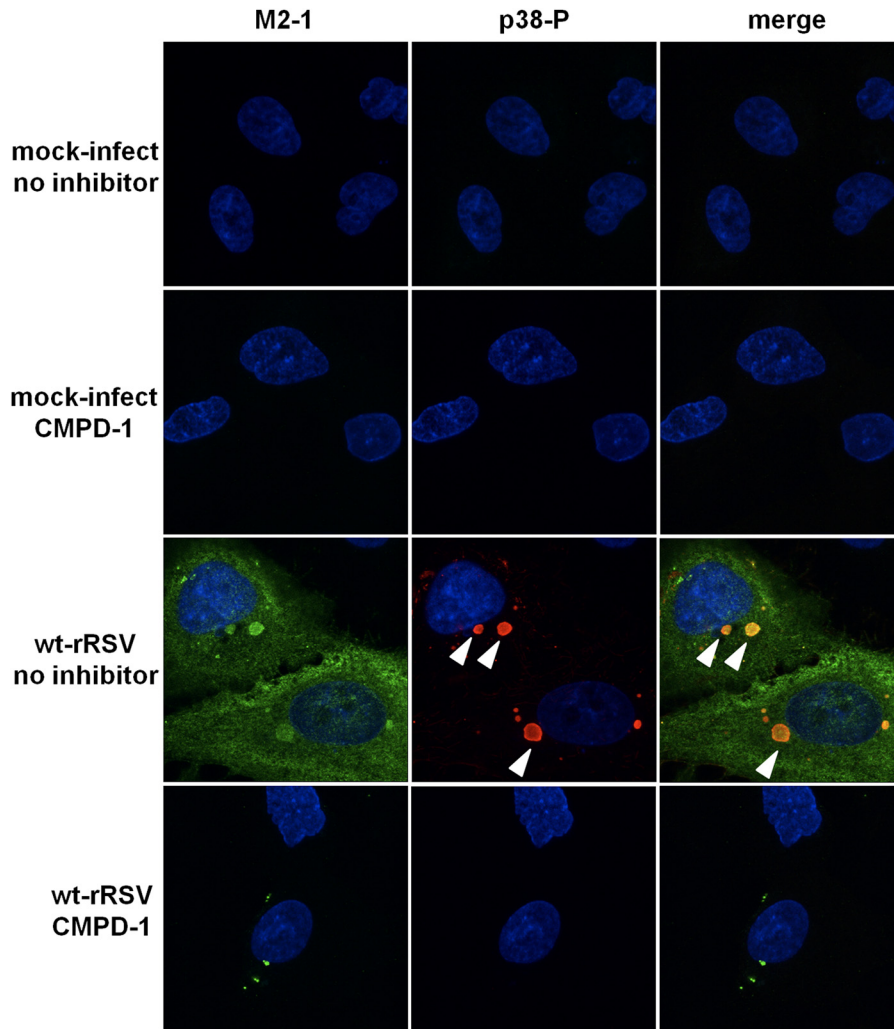


FIG 3 Immunofluorescence images of the intracellular distribution of p38-P and the viral M2-1 protein in response to RSV infection and treatment with inhibitor CMPD-1. Monolayers of A549 cell were infected with wt-rRSV at an MOI of 0.5 or were mock infected. The cells were treated with the inhibitor CMPD-1 or mock treated 75 min after infection, incubated for a total of 18 h, fixed, and immunostained using antibodies specific to M2-1 (green) and p38-P (red), and the nuclei were stained with DAPI (blue). The white arrowheads indicate examples of IBs.

reduced equally to avoid saturation of the more intense signals). In contrast, in RSV-infected cells, OGT was readily detected in dense cytoplasmic bodies. These bodies were found to contain dense accumulation of the RSV P (Fig. 7A) and M2-1 (Fig. 8A) proteins and thus were IBs. This indicated that similar to p38-P, OGT was sequestered in IBs during RSV infection.

TIA-1 also was present in a diffuse distribution in mock-infected cells, indicating the absence of SGs (Fig. 7A and 8A). When mock-infected cells were treated with arsenite for 30 min, the formation of SGs, revealed as intense speckles containing TIA-1, was evident (Fig. 7A and 8A). The distribution of TIA-1 also was diffuse in the majority of RSV-infected cells, indicating a lack of SGs in most cases. Treatment of RSV-infected cells with arsenite resulted in the appearance of aggregates of TIA-1, indicative of SGs. In addition, the arsenite treatment resulted in IBs that were smaller and more numerous than in non-arsenite-treated cells, as already noted (Fig. 7A and 8A). The appearance of SGs in RSV-infected cells following arsenite treatment indicated at least a partial recovery of OGT function.

In arsenite-treated RSV-infected cells, the IBs and SGs were scattered in the cytoplasm, with no apparent colocalization (Fig. 7A and 8A). The RSV P protein showed clear spatial segregation with the IBs but did not colocalize with the SGs (Fig. 7A). The RSV M2-1 protein was similarly present in IBs but, surprisingly, was also found colocalized with TIA-1 in the SGs that formed in response to arsenite treatment (Fig. 8A). The lack of colocalization of IBs and SGs, and the difference between the P and M2-1 proteins with regard to colocalization with SGs, was further illustrated by cross-sectional analysis and three-dimensional modeling of the fluorescence confocal images, shown both as selected images (Fig. 7B and 8B, respectively) and as animations (see Videos SA and SB, respectively, in the supplemental material). Thus, when SGs formed in RSV-infected cells following arsenite treatment, the M2-1 protein translocated to the newly forming SGs. Whether the SG-associated M2-1 protein was derived from IBs or had been free in the cytoplasm is unknown.

To further investigate the effect of OGT sequestration within the viral IBs, we investigated the intracellular distribu-

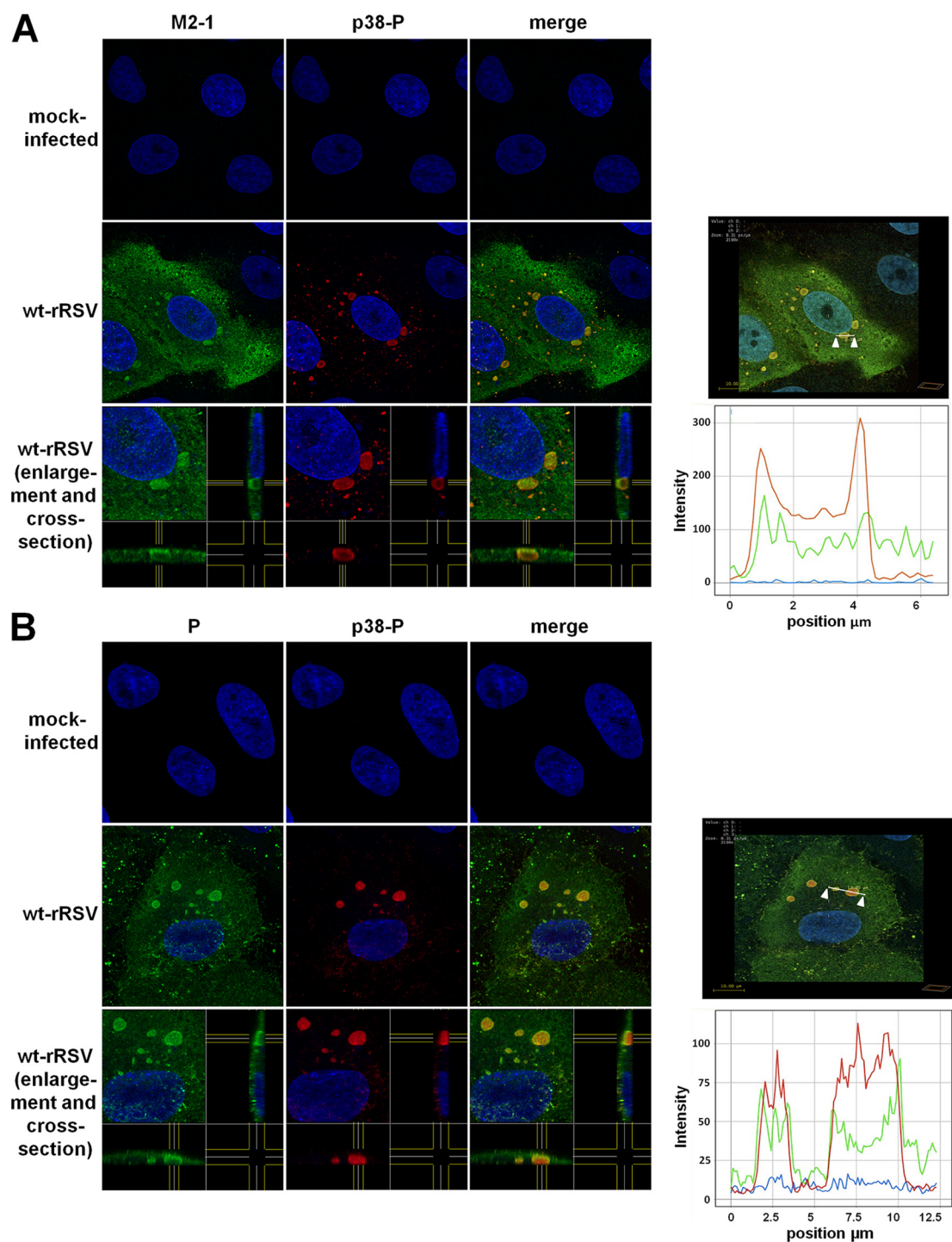
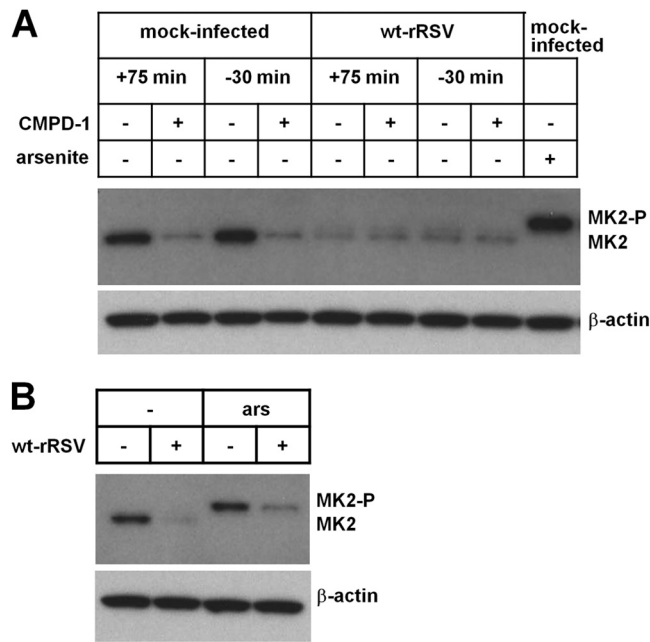


FIG 4 Immunofluorescence imaging and intensity profiles of viral IBs. A549 cells were infected with wt-rRSV at an MOI of 0.5 or were mock infected. At 18 h postinfection, the cells were fixed and stained with antibodies for either the viral M2-1 (A, green) or P (B, green) protein and p38-P (red). Nuclei were stained with DAPI (blue). The samples were analyzed by confocal microscopy. In panels A and B, the bottom row of images shows enlargements from the middle row as well as cross-sections in the x and y dimensions. The panels on the right show a single mid-cell layer from a z-stack of confocal images (top images). The white line with arrowheads below each end indicates the track of a line intensity profile across one (A) or two (B) selected IBs (bottom images).

tion of OGN, marking the locations of proteins that had been modified by OGT. A549 cells were infected or mock infected in the same way as in previous experiments, and at 18 h postinfection immunofluorescence was performed with antibodies

against RSV, OGT, and OGN (Fig. 9) or with RSV, OGN, and the SG marker eIF3 (Fig. 10). In these experiments, limitations in the available primary and secondary antibodies precluded the use of murine antibodies that were monospecific to RSV P



or M2-1, and instead we used polyspecific goat antibodies against RSV virions; as a result, RSV-specific staining was not limited to IBs.

In mock-infected cells, OGT was distributed diffusely (Fig. 9A; the diffuse pattern is not visible because the signal intensities of all of the images were reduced equally to avoid saturation of the more intense signals). In the same cells, OGN was faintly detected, with small punctate spots and diffuse patches in the cytoplasm. When mock-infected cells were treated with arsenite, the distribution of OGT was not detectably changed, but OGN was evident in a large number of cytoplasmic aggregates (Fig. 9A), indicating the enzymatic activity of OGT. Immunostaining for eIF3 identified these aggregates as SGs (Fig. 10).

In RSV-infected cells, OGT was concentrated in IBs, as already noted (Fig. 7 and 8), whereas the accumulation of OGN was diffuse and similar to that in mock-infected cells (Fig. 9A). Arsenite treatment of RSV-infected cells resulted in the accumulation of OGN in SGs, identified by colocalization with eIF3 (Fig. 10). The confocal images of arsenite-treated, RSV-infected cells from Fig. 9A and 10A were illustrated by cross-sectional analysis and reconstructed as three-dimensional images, shown in Fig. 9B and 10B, respectively. This further illustrated that OGN showed clear colocalization with eIF3 in SGs (Fig. 10B), whereas OGT did not colocalize with SGs (Fig. 9B), as already shown.

These results showed that RSV infection resulted in the sequestration of OGT in viral IBs but that the size of the IBs was greatly

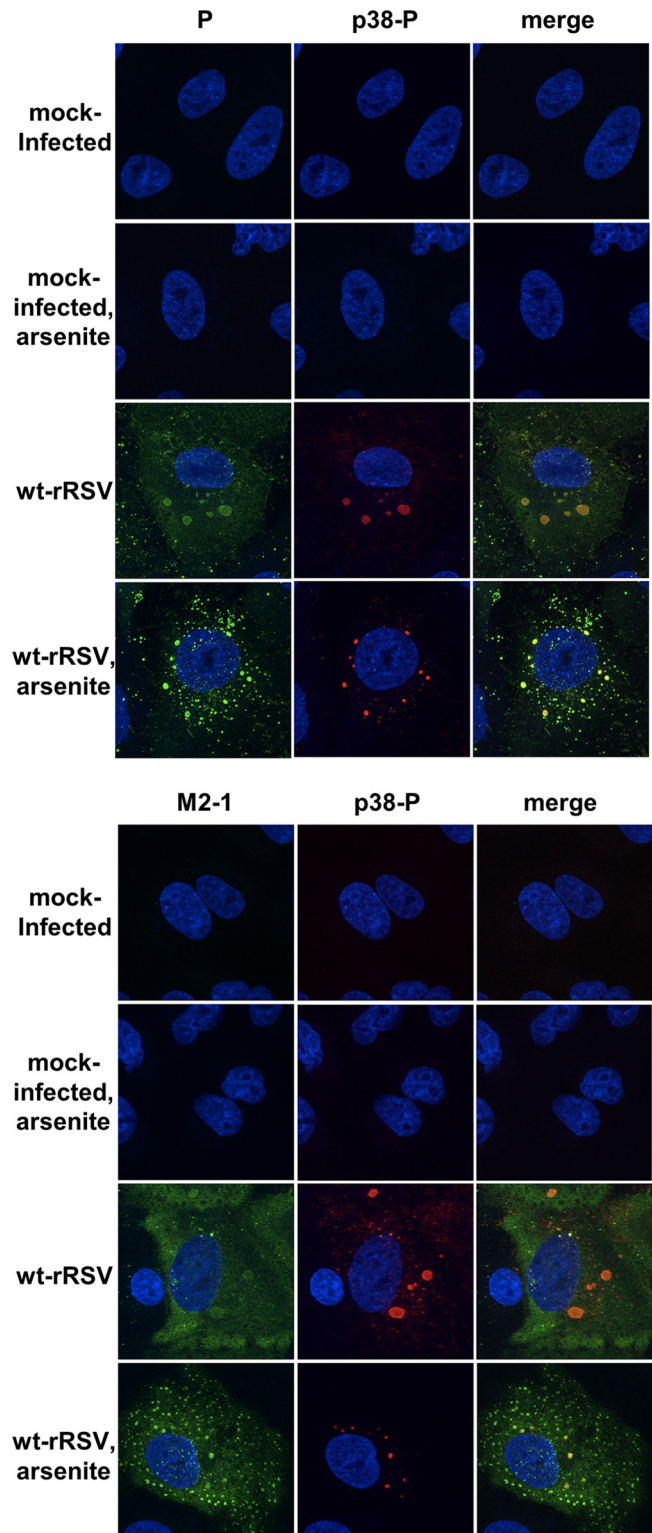


FIG 6 Immunofluorescence analysis of the intracellular distribution of p38-P and viral P (A) or M2-1 (B) protein in response to RSV infection and treatment with arsenite. Monolayer cultures of A549 cells were infected with wt-rRSV at an MOI of 0.5 or were mock infected. Cultures were treated with arsenite or mock treated for 30 min at 18 h postinfection, fixed, and immunostained using antibodies to the P (A, green) or M2-1 (B, green) protein and p38-P (red). Nuclei were stained with DAPI (blue). Samples were analyzed by confocal microscopy.

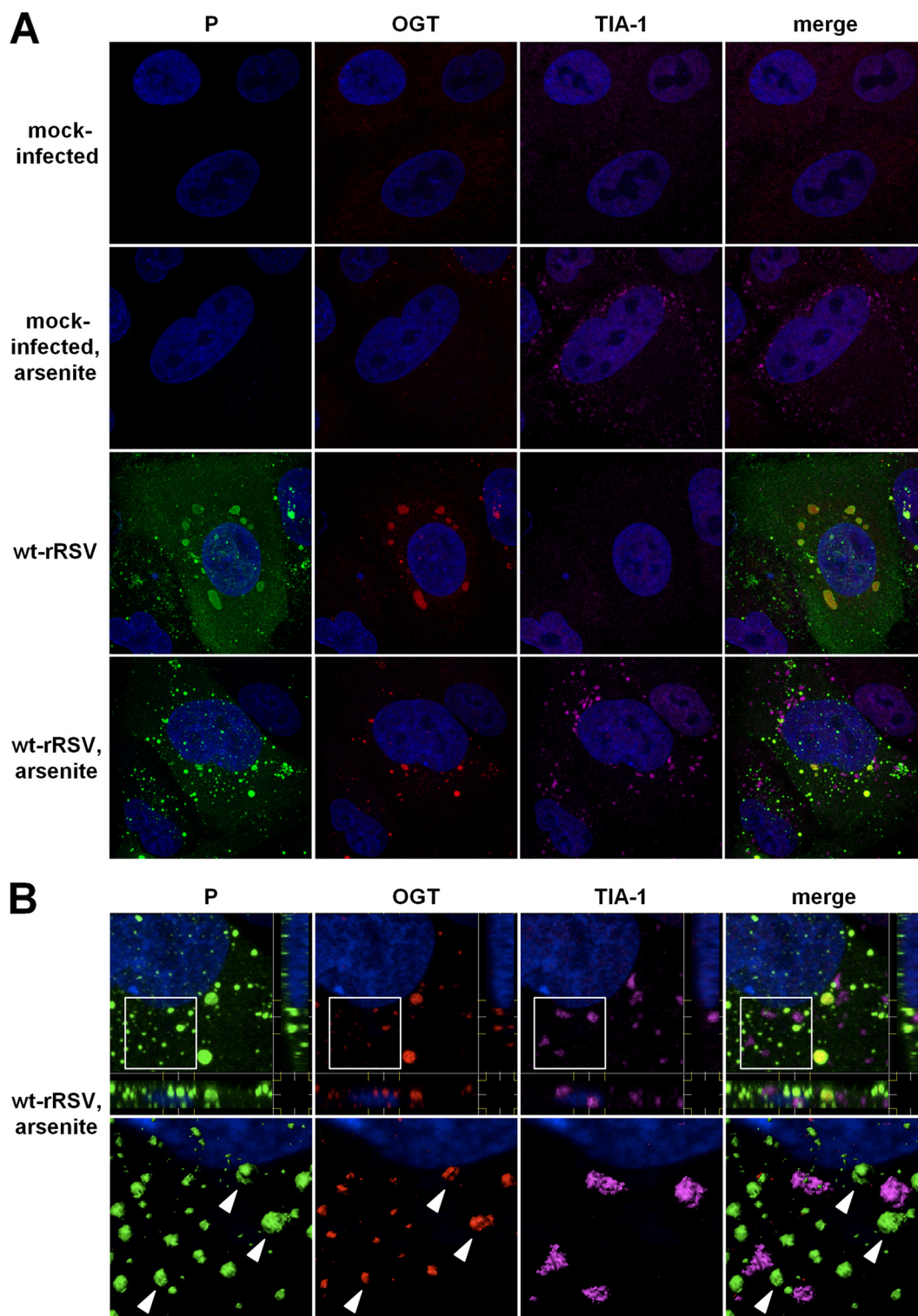


FIG 7 Immunofluorescence analysis of the intracellular distribution of OGT, the viral P protein, and the SG marker TIA-1 in response to RSV infection and treatment with arsenite. Monolayer cultures of A549 cells were infected with wt-rRSV at an MOI of 0.5 or were mock infected. Cultures were treated with arsenite or mock treated for 30 min at 18 h postinfection, fixed, and immunostained using antibodies specific to the P protein (green), OGT (red), and TIA-1 (violet), and nuclei were stained with DAPI (blue). Panel B shows enlargements from the bottom row of panel A, with further enlargements rendered as three-dimensional images. White arrowheads in panel B indicate representative IBs, illustrating that the IBs contain P and OGT but do not localize with TIA-1. An animation of panel B is shown in Video SA in the supplemental material.

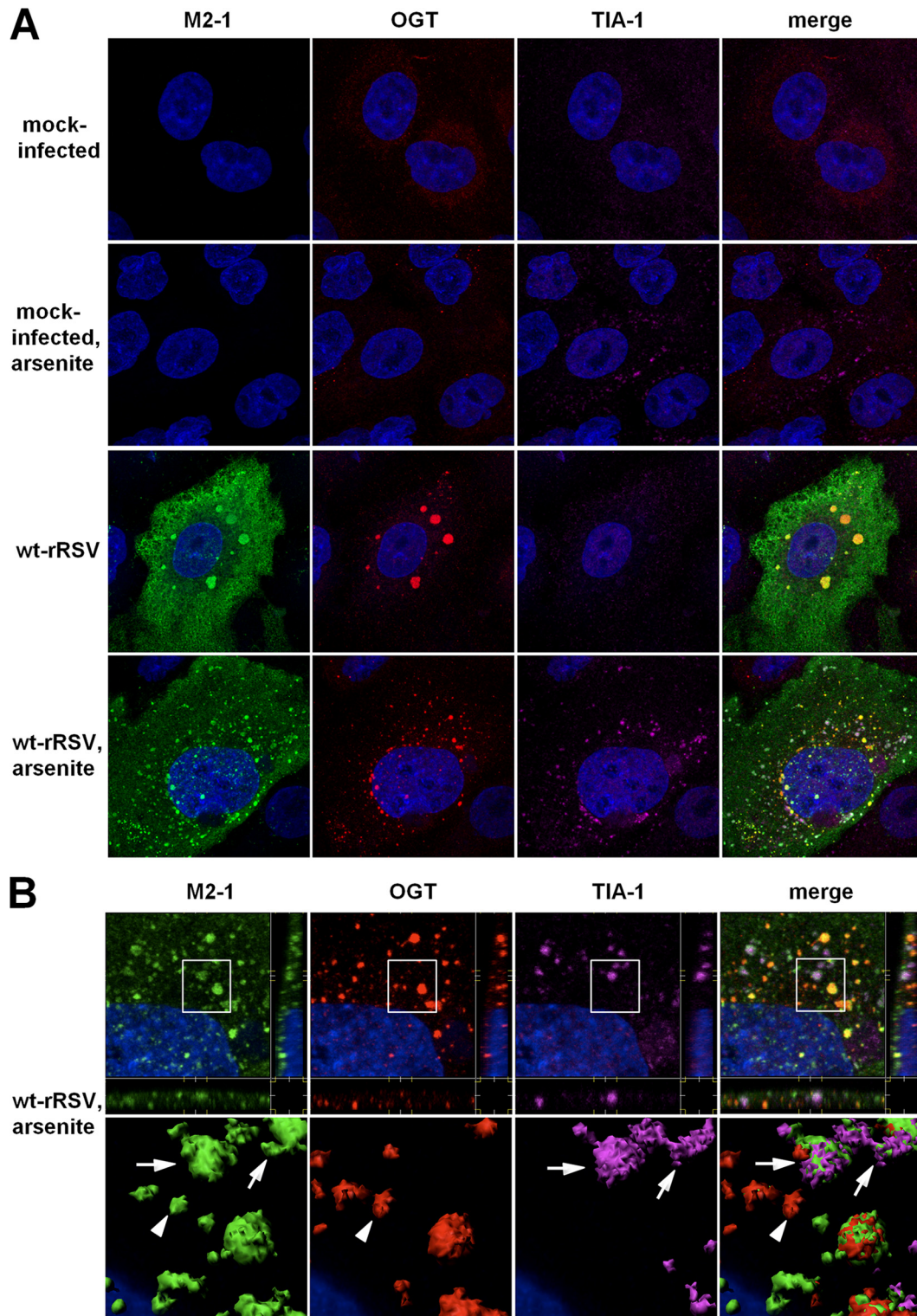


FIG 8 Immunofluorescence analysis of the intracellular distribution of OGT, the viral M2-1 protein, and the SG marker TIA-1 in response to RSV infection and treatment with arsenite. Monolayer cultures of A549 cells were infected with wt-rRSV at an MOI of 0.5 or were mock infected. Cultures were treated with arsenite or mock treated for 30 min at 18 h postinfection, fixed, and immunostained using antibodies specific to M2-1 (green), OGT (red), and TIA-1 (violet), and nuclei were stained with DAPI (blue). Panel B shows enlargements from the bottom row of panel A, with further enlargements rendered as three-dimensional images. The white arrowhead in panel B indicates a representative IB containing M2-1 and OGT, but not TIA-1, and the white arrows in panel B indicate representative SGs containing M2-1 and TIA-1. An animation of panel B is shown in Video SB in the supplemental material.

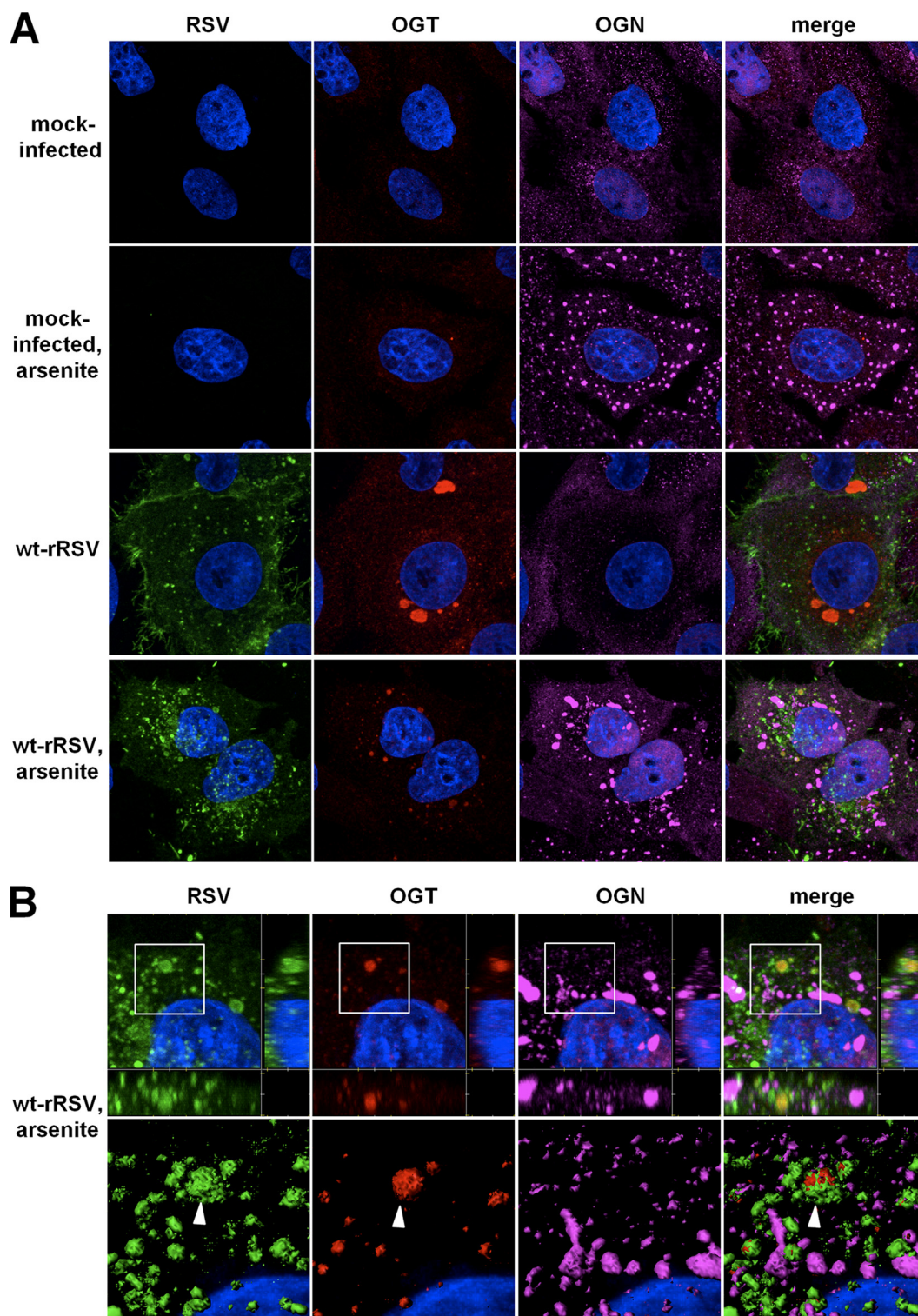


FIG 9 Immunofluorescence analysis of the intracellular distribution of OGT and OGN in response to RSV infection and treatment with arsenite. Monolayer cultures of A549 cells were infected with wt-rRSV at an MOI of 0.5 or were mock infected. Cultures were treated with arsenite or mock treated for 30 min at 18 h postinfection, fixed, and immunostained using antibodies against RSV (green), OGT (red), and OGN (violet). Nuclei were stained with DAPI (blue). Panel B shows enlargements from the bottom row of panel A, with further enlargements rendered as three-dimensional images. Incidentally, the anti-RSV antibodies used in this particular experiment had been raised against whole virus and RSV staining was not limited to IBs; thus, colocalization of viral protein with OGT in IBs (one example is indicated by a white arrowhead in panel B) was much less evident than in other experiments.

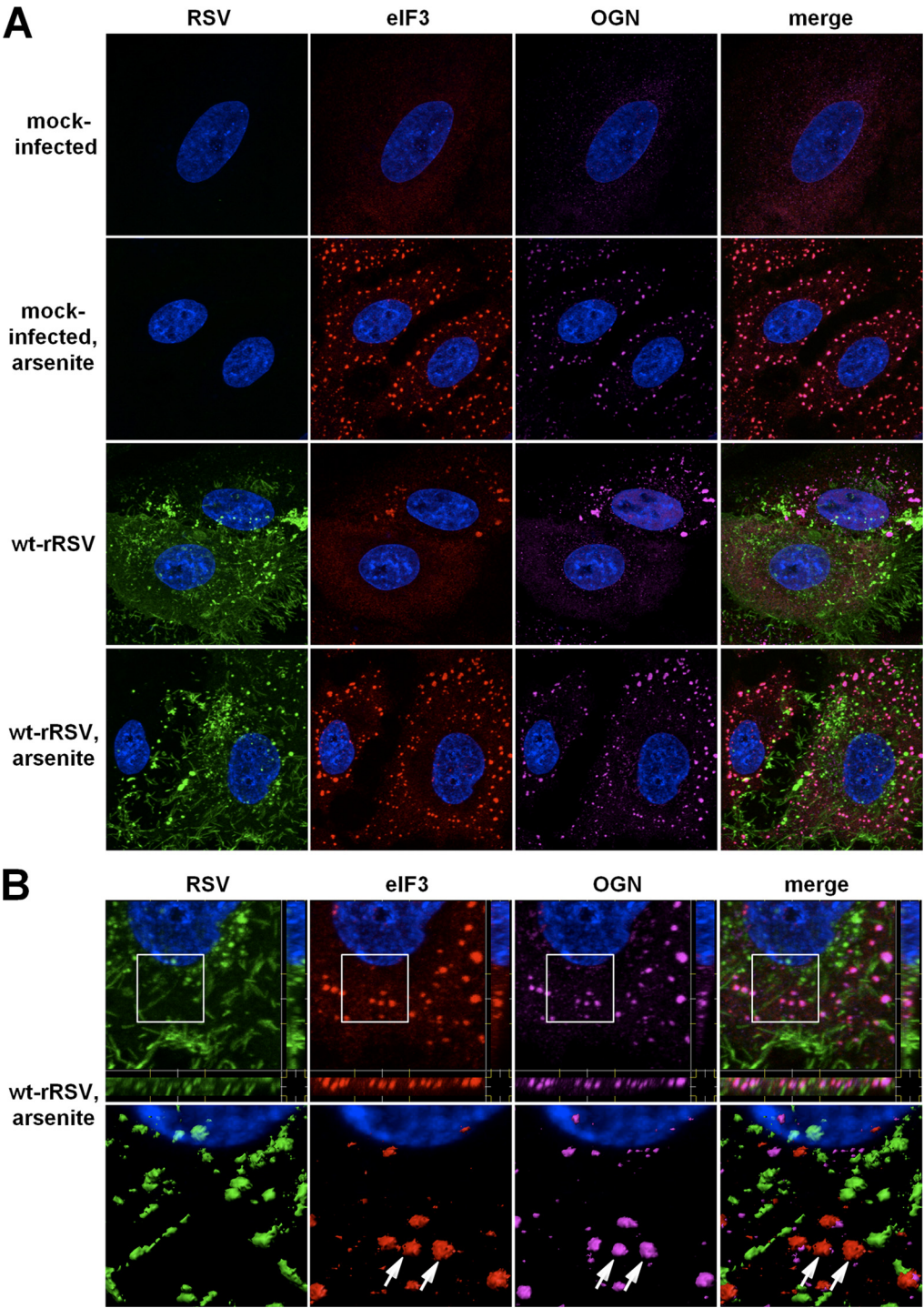


FIG 10 Immunofluorescence analysis of the intracellular distribution of SGs and OGN in response to RSV infection and treatment with arsenite. Monolayer cultures of A549 cells were infected with wt-rRSV at an MOI of 0.5 or were mock infected. Cultures were treated with arsenite or mock treated for 30 min at 18 h postinfection, fixed, and immunostained using antibodies against RSV (green), the SG marker eIF3 (red), and OGN (violet). Nuclei were stained with DAPI (blue). Panel B shows enlargements from the bottom row of panel A, with further enlargements rendered as three-dimensional images. White arrows in panel B show examples of colocalization of eIF3 and OGN, indicating that both are in SGs.

diminished by the induction of severe oxidative stress by a brief arsenite treatment. Thus, the sequestration appeared to be reversible. Our data did not reveal any discernible differences in the spatial localization of proteins modified by the addition of OGN

in mock- versus RSV-infected cells, although the species of proteins that are OGN modified may differ under these two conditions and merit further investigation.

Negative association between IBs and SGs. We noted that

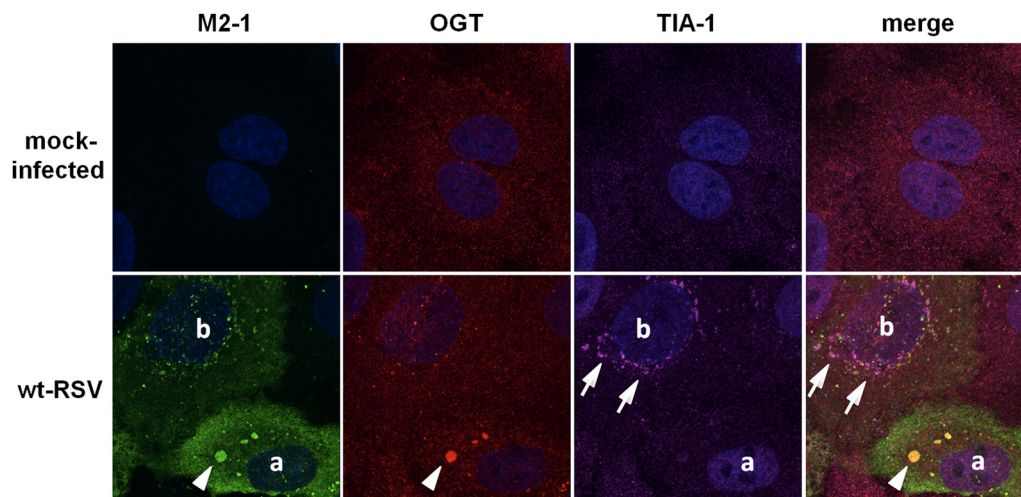


FIG 11 Examples of RSV-infected cells that contain IBs alone or IBs and SGs. Monolayer cultures of A549 cells were infected with wt-rRSV at an MOI of 0.5 or were mock infected. At 18 h postinfection, cells were fixed and immunostained using antibodies specific for M2-1 (green), OGT (red), and TIA-1 (violet). Nuclei were stained with DAPI (blue). White arrowheads indicate an example of a well-developed IB; white arrows indicate areas of SGs. The cell labeled “a” is an example of an RSV-infected cell that contains well-developed IBs and lacks detectable SGs; this pattern was observed in ~95% of RSV-infected cells. The cell labeled “b” is an example of an RSV-infected cell in which the IBs are smaller and SGs also are present; this pattern was observed in ~5% of RSV-infected cells.

RSV-infected cells that contained well-developed, large IBs did not have detectable SGs, as is illustrated in Fig. 11 with the cell marked “a.” In contrast, a small fraction of RSV-infected cells were found to contain small IBs, and these cells also contained SGs, as is illustrated in Fig. 11 with the cell marked “b.” We quantified the relative abundance of these two phenotypes in A549 cells that were infected with RSV at an MOI of 0.5 PFU per cell and analyzed 18 h postinfection (as in all of the experiments in this study). Two replicate experiments were performed: in each, 25 microscopic fields were counted, with a total of approximately 300 RSV-infected cells. The percentages of infected cells with SGs in the two experiments were 5.8% and 4.3%. Thus, most RSV-infected cells formed large, prominent IBs that apparently precluded SG formation, whereas a small fraction of infected cells formed smaller IBs that permitted SG formation. The pattern of small, numerous IBs present in this small subpopulation of RSV-infected cells was similar in appearance to the pattern that was induced in the majority of RSV-infected cells by brief arsenite treatment (Fig. 7 and 8): in each case, the presence of small IBs was associated with the presence of SGs, and there was a negative association between large, prominent IBs and SGs.

DISCUSSION

The MAPKs, including p38 MAPK, ERK, and Jun N-terminal protein kinase (JNK), represent interrelated pathways involved in cellular homeostasis and responses to external stimuli, including viral infection. Previous evidence indicated roles for p38 MAPK and ERK, in particular, in RSV infection (11, 12, 34). Our study demonstrated that RSV interferes with the p38 signaling pathway by spatially sequestering p38-P into viral IBs. p38 has been shown to be indispensable in the stress- and cytokine-dependent activation of MK2. In addition, the tight binding between MK2 and p38 is required for the stable accumulation of both proteins (20, 21). Consistent with this, one of the outcomes of the sequestration of p38-P in RSV IBs in the present study was the extensive depletion of MK2, effectively achieving an MK2 knockdown in RSV-in-

fected cells. MK2 has been shown to be an essential component in the inflammatory response. For example, inactivation of the mouse MK2 gene by a targeted mutation resulted in severely reduced production of TNF- α and IFN- γ and significantly reduced production of IL-1 β , IL-6, and IL-10 in response to lipopolysaccharide stimulation (16). Many of these proinflammatory proteins are encoded by mRNAs marked for rapid degradation by AREs found in their 3' untranslated regions (UTRs), and the activation of p38/MK2 pathway results in the stabilization of these ARE-containing mRNAs (15, 17, 35). Specifically, activated MK2 mediates phosphorylation of the cellular zinc finger protein tristetrapolin (TTP). While unphosphorylated TTP binds to and promotes the degradation of ARE-containing mRNAs, phosphorylation of TTP by MK2 promotes complex formation between TTP-P and the chaperone protein 14-3-3, which excludes TTP from SGs and thereby inhibits TTP-dependent degradation of ARE-containing mRNA (13, 36). Thus, viral interference with signal transduction through p38 leading to MK2 depletion would reduce the production of anti-inflammatory and antiviral factors.

We also showed that RSV infection resulted in the sequestration into viral IBs of another key player in intracellular signaling, OGT. OGT catalyzes posttranslational attachment of single OGN molecules to serine and threonine residues of cellular proteins in a dynamic interplay with their phosphorylation status, thereby altering protein stability, interactions, spatial distribution, and activity. In particular, OGT is known to be involved in modifying the translation machinery during stress induction by supporting the assembly of SGs and processing bodies (25, 26). SGs are not constitutively present in cells but can form under conditions of environmental stress or infection. They are complex cytoplasmic foci that contain stalled translation complexes that subsequently can be directed for translation or degradation. Thus, SGs play an important role in posttranscriptional control of gene expression and have particular importance for ARE-containing mRNAs, including those of proinflammatory and antiviral cytokines and other proteins. Sequestration of OGT in IBs would presumably preclude

its role in cellular regulation and, in particular, would prevent OGT from triggering the formation of SGs.

The sequestration of both p38-P and OGT into RSV IBs appeared to be partly reversed by oxidative stress induced by a brief treatment with arsenite. In both cases, this led to an apparent shrinkage and fragmentation of the IBs. Furthermore, arsenite treatment was associated with the activation of the remaining MK2, as well as the formation of SGs and the addition of OGN to target proteins within SGs. This suggested that the apparent fragmentation of IBs in response to arsenite treatment may have resulted in the release of p38-P and OGT; if so, this indicates that these proteins had been transported to IBs and sequestered but had not been damaged. Arsenite disrupts ATP production, among other things, and its ability to reduce and scatter IBs and release p38-P and OGT suggests that the maintenance of IBs and the sequestration of p38-P and OGT are highly dynamic processes that require energy.

Examination of RSV-infected A549 cells showed that ~95% of infected cells contained prominent IBs with no detectable SGs, whereas the remaining ~5% of infected cells contained smaller IBs as well as SGs. This suggests that the formation of large, prominent IBs precludes the formation of SGs. This could be explained by the observed efficient sequestration of OGT by large IBs, making OGT unavailable to induce SGs. In contrast, in the few infected cells in which IB formation was less developed, sequestration of OGT was less prominent, leaving free OGT available to induce SG formation. This suggests that RSV infection is a stimulus for SG formation, but this normally is blocked by virus-mediated sequestration of OGT. In the small fraction of RSV-infected cells that contained smaller IBs as well as SGs, the formation of large IBs may have been delayed or reduced, perhaps due to delayed or reduced viral replication in those particular cells. This might result from variability in the cell population, including factors such as host defense or permissiveness to infection, variability in the virus population, including the presence of defective interfering particles in those cells, or other stochastic factors.

Several recent studies have noted SGs in the context of RSV infection (8, 30, 37). Lindquist et al. reported SG formation in RSV-infected cells and suggested that SGs enhanced RSV replication (8). However, they observed that SGs occurred in only a small percentage of RSV-infected cells: for example, at an MOI of 1, only approximately 10% of the infected cells contained SGs at 16 h postinfection (8), which is similar to the findings in the present report (i.e., ~5% of cells at 18 h postinfection with an MOI of 0.5). Thus, the formation of SGs does not appear to be a regular feature of RSV-infected cells, and the association of SGs with enhanced RSV replication was not confirmed in a subsequent study (38). Lindquist et al. reported that the size of the IBs was larger in the small fraction of cells containing SGs than in the large fraction of cells lacking SGs. However, this size difference was small, with an average IB volume of ~0.4 μm^3 in infected cells without SGs to ~0.6 μm^3 in infected cells with SGs, which translates to an average radius of ~0.4 μm versus ~0.5 μm . In the present work, we observed that the large majority of RSV-infected cells contained large, prominent IBs and did not contain SGs. These large IBs ranged in size between 2 and 3 μm in radius and thus were far bigger than the ones described by Lindquist et al. We observed dense accumulation of OGT in these large IBs, suggesting that they were very efficient in sequestering OGT and thereby inhibiting SG formation. The reason for the difference in IB size between

the report of Lindquist et al. and the present study is not clear. It may be relevant that the measurements were taken at different times during infection: our study focused on 18 h postinfection, which is at or slightly following the peak of viral RNA expression, when the effects of IBs on RSV replication might be the most relevant, whereas the measurements of Lindquist et al. were made at a later time, 24 h postinfection. Lindquist et al. documented a substantial increase in SG formation at this late time point, and it may be that the cells were experiencing increased stress due to the well-advanced viral infection, which may have affected IB size, among other things.

Hanley et al. also described SGs in the context of RSV infection (30). This study similarly showed that SGs formed in only a small percentage (~5%) of cells infected with wild-type RSV, whereas SGs were much more frequent in cells infected with an RSV mutant that lacked most of the trailer region and exhibited reduced replication. These results are consistent with the present study: specifically, both studies suggest that RSV infection has the potential to induce SG formation but that the wild-type virus suppresses this induction. It may be that the trailer sequence that is missing in the mutant RSV of Hanley et al. is important for suppressing SG formation because of reduced replication and hence reduced expression of viral proteins. In any event, our work differs from these previous studies in providing a mechanism for how RSV suppresses SG formation, namely, by the sequestration of OGT, an upstream regulatory molecule in SG assembly, into the viral IBs.

Several other recent studies had noted an association between host cell molecules and RSV IBs. In the first of these reports, Brown et al. noted the appearance of heat shock protein Hsp70 within virus-induced IBs (9). Lindquist et al. also made the interesting observation that HuR, a component of SGs, localized to IBs during RSV infection, although this did not appear to contribute to RSV infection, since knockdown of HuR had no effect on viral replication (8). Another recent study that was published while the manuscript for this article was in preparation provided evidence of the sequestration of additional cellular proteins in IBs, specifically, melanoma differentiation-associated gene 5 (MDA5) protein and mitochondrial antiviral signaling (MAVS) protein (39). This was associated with suppression of IFN- β production. Our present results provide evidence that the sequestration of components of innate immune response systems and signal transduction pathways into viral IBs is a prominent feature of RSV infection (and, by analogy, possibly for other viruses, such as human metapneumovirus and measles virus, that also form viral IBs).

The observation that RSV targets and sequesters p38 and OGT is particularly noteworthy because these proteins may have a broad impact on host cell signaling and affect a wide range of cellular activities beyond the stability of ARE-containing mRNAs and the formation of SGs, including a myriad of other targets that are necessary for viral translation (40) and regulation of the adaptive immune response (41). For example, p38 activates many other protein kinases in addition to MK2, including MK3, MK5, MSK1/2, and MNK1. Moreover, transcription factors such as ATF-2, SAP1, CHOP, STAT1, NFAT, GADD135, and numerous others also are downstream substrates of p38 phosphorylation (42). Similarly, OGN-modified proteins affect a variety of cellular functions, including transcription, translation, protein processing, growth, metabolism, stress, and the immune response (40, 41, 43–45). As a specific example, under IL-1 induction or osmotic

stress, OGN modification of TAB1 has been shown to modulate TAK1 activation, leading to I κ B kinase (IKK) phosphorylation and NF- κ B translocation (46). By confining OGT, RSV could potentially prevent the activation of TAB1/TAK1 pathway and therefore influence NF- κ B-induced cytokine production.

We were surprised to find that following arsenite treatment, the viral M2-1 protein appeared in SGs. M2-1 was previously shown to function as a viral elongation/anti-termination factor that is necessary for the synthesis of full-length viral mRNAs and is essential for RSV replication (47). M2-1 contains a Cys₃-His₁ (CCCH) motif that is essential for its function in viral RNA synthesis (48, 49). Interestingly, it was previously noted that this CCCH motif is a feature that M2-1 shares with TTP (48, 49). The present study takes this analogy further by showing that like TTP, M2-1 can be recruited to SGs. This raises the possibility that M2-1 may have TTP-related roles in affecting SG formation and activity and RNA metabolism. This is under investigation.

In summary, we found that p38 and OGT, two key cellular molecules that are centrally involved in posttranslational protein modification and signal transduction, are sequestered inside RSV IBs during infection. Given the wide-ranging roles of these cellular proteins, their sequestration has the potential to substantially affect cellular activities during RSV infection. In the present study, we showed that this resulted in suppression of SG formation and was an active, reversible process. Future work is needed to study the full impact of p38/OGT sequestration and to identify additional host molecules that may be sequestered during RSV infection. Furthermore, this work identified an interaction between the viral M2-1 protein and SGs that potentially suggests a TTP-related role for this viral protein.

ACKNOWLEDGMENTS

We thank Juraj Kabat from the NIAID Research and Technologies Branch for his invaluable help with postimage analysis.

This work was supported by the Intramural Research Program of the NIAID, NIH.

REFERENCES

- Collins PL, Graham BS. 2008. Viral and host factors in human respiratory syncytial virus pathogenesis. *J. Virol.* 82:2040–2055.
- Storey S. 2010. Respiratory syncytial virus market. *Nat. Rev. Drug Discov.* 9:15–16.
- Derdowski A, Peters TR, Glover N, Qian R, Utley TJ, Burnett A, Williams JV, Spearman P, Crowe JE, Jr. 2008. Human metapneumovirus nucleoprotein and phosphoprotein interact and provide the minimal requirements for inclusion body formation. *J. Gen. Virol.* 89:2698–2708.
- García J, García-Barreno B, Vivo A, Melero JA. 1993. Cytoplasmic inclusions of respiratory syncytial virus-infected cells: formation of inclusion bodies in transfected cells that coexpress the nucleoprotein, the phosphoprotein, and the 22K protein. *Virology* 195:243–247.
- Spehner D, Kirn A, Drillien R. 1991. Assembly of nucleocapsidlike structures in animal cells infected with a vaccinia virus recombinant encoding the measles virus nucleoprotein. *J. Virol.* 65:6296–6300.
- Carromeu C, Simabuco FM, Tamura RE, Farinha Arcieri LE, Ventura AM. 2007. Intracellular localization of human respiratory syncytial virus L protein. *Arch. Virol.* 152:2259–2263.
- García-Barreno B, Delgado T, Melero JA. 1996. Identification of protein regions involved in the interaction of human respiratory syncytial virus phosphoprotein and nucleoprotein: significance for nucleocapsid assembly and formation of cytoplasmic inclusions. *J. Virol.* 70:801–808.
- Lindquist ME, Lifland AW, Utley TJ, Santangelo PJ, Crowe JE, Jr. 2010. Respiratory syncytial virus induces host RNA stress granules to facilitate viral replication. *J. Virol.* 84:12274–12284.
- Brown G, Rixon HW, Steel J, McDonald TP, Pitt AR, Graham S, Sugrue RJ. 2005. Evidence for an association between heat shock protein 70 and the respiratory syncytial virus polymerase complex within lipid-raft membranes during virus infection. *Virology* 338:69–80.
- Harris J, Werling D. 2003. Binding and entry of respiratory syncytial virus into host cells and initiation of the innate immune response. *Cell. Microbiol.* 5:671–680.
- Marchant D, Singhera GK, Utokaparch S, Hackett TL, Boyd JH, Luo ZS, Si XN, Dorscheid DR, McManus BM, Hegele RG. 2010. Toll-like receptor 4-mediated activation of p38 mitogen-activated protein kinase is a determinant of respiratory virus entry and tropism. *J. Virol.* 84:11359–11373.
- Monick M, Staber J, Thomas K, Hunninghake G. 2001. Respiratory syncytial virus infection results in activation of multiple protein kinase C isoforms leading to activation of mitogen-activated protein kinase. *J. Immunol.* 166:2681–2687.
- Gaestel M. 2006. MAPKAP kinases—MKs—two's company, three's a crowd. *Nat. Rev. Mol. Cell Biol.* 7:120–130.
- Zarubin T, Han J. 2005. Activation and signaling of the p38 MAP kinase pathway. *Cell Res.* 15:11–18.
- Bakheet T, Frevel M, Williams BR, Greer W, Khabar KS. 2001. ARED: human AU-rich element-containing mRNA database reveals an unexpectedly diverse functional repertoire of encoded proteins. *Nucleic Acids Res.* 29:246–254.
- Kotlyarov A, Neininger A, Schubert C, Eckert R, Birchmeier C, Volk HD, Gaestel M. 1999. MAPKAP kinase 2 is essential for LPS-induced TNF- α biosynthesis. *Nat. Cell Biol.* 1:94–97.
- Winzen R, Kracht M, Ritter B, Wilhelm A, Chen CY, Shyu AB, Muller M, Gaestel M, Resch K, Holtmann H. 1999. The p38 MAP kinase pathway signals for cytokine-induced mRNA stabilization via MAP kinase-activated protein kinase 2 and an AU-rich region-targeted mechanism. *EMBO J.* 18:4969–4980.
- Lukas SM, Kroe RR, Wildeson J, Peet GW, Frego L, Davidson W, Ingraham RH, Pargellis CA, Labadia ME, Werneburg BG. 2004. Catalysis and function of the p38 α .MK2a signaling complex. *Biochemistry* 43:9950–9960.
- White A, Pargellis CA, Studts JM, Werneburg BG, Farmer BT, II. 2007. Molecular basis of MAPK-activated protein kinase 2:38 assembly. *Proc. Natl. Acad. Sci. U. S. A.* 104:6353–6358.
- Kotlyarov A, Yannoni Y, Fritz S, Laass K, Telliez JB, Pitman D, Lin LL, Gaestel M. 2002. Distinct cellular functions of MK2. *Mol. Cell. Biol.* 22:4827–4835.
- Sudo T, Kawai K, Matsuzaki H, Osada H. 2005. p38 mitogen-activated protein kinase plays a key role in regulating MAPKAPK2 expression. *Biochem. Biophys. Res. Commun.* 337:415–421.
- Clifton AD, Young PR, Cohen P. 1996. A comparison of the substrate specificity of MAPKAP kinase-2 and MAPKAP kinase-3 and their activation by cytokines and cellular stress. *FEBS Lett.* 392:209–214.
- Beardmore VA, Hinton HJ, Eftychi C, Apostolaki M, Armaka M, Darragh J, McIlrath J, Carr JM, Armit LJ, Clacher C, Malone L, Kollias G, Arthur JS. 2005. Generation and characterization of p38beta (MAPK11) gene-targeted mice. *Mol. Cell. Biol.* 25:10454–10464.
- Newbury SF, Muhlemann O, Stoecklin G. 2006. Turnover in the Alps: an mRNA perspective. *Workshops on mechanisms and regulation of mRNA turnover. EMBO Rep.* 7:143–148.
- Ohn T, Anderson P. 2010. The role of posttranslational modifications in the assembly of stress granules. *Wiley Interdiscip. Rev. RNA* 1:486–493.
- Ohn T, Kedersha N, Hickman T, Tisdale S, Anderson P. 2008. A functional RNAi screen links O-GlcNAc modification of ribosomal proteins to stress granule and processing body assembly. *Nat. Cell Biol.* 10:1224–1231.
- White JP, Lloyd RE. 2012. Regulation of stress granules in virus systems. *Trends Microbiol.* 20:175–183.
- Cheung WD, Hart GW. 2008. AMP-activated protein kinase and p38 MAPK activate O-GlcNAcylation of neuronal proteins during glucose deprivation. *J. Biol. Chem.* 283:13009–13020.
- Giot L, Bader JS, Brouwer C, Chaudhuri A, Kuang B, Li Y, Hao YL, Ooi CE, Godwin B, Vitols E, Vijayadamar G, Pochart P, Machineni H, Welsh M, Kong Y, Zerhusen B, Malcolm R, Varrone Z, Collis A, Minto M, Burgess S, McDaniel L, Stimpson E, Spriggs F, Williams J, Neurath K, Ioime N, Agee M, Voss E, Furtak K, Renzulli R, Aanensen N, Carrola S, Bickelhaupt E, Lazovatsky Y, DaSilva A, Zhong J, Stanyon CA, Finley RL, Jr, White KP, Braverman M, Jarvie T, Gold S, Leach M, Knight J, Shimkets RA, McKenna MP, Chant J, Rothberg JM. 2003. A

- protein interaction map of *Drosophila melanogaster*. *Science* 302:1727–1736.
30. Hanley LL, McGivern DR, Teng MN, Djang R, Collins PL, Fearn R. 2010. Roles of the respiratory syncytial virus trailer region: effects of mutations on genome production and stress granule formation. *Virology* 406:241–252.
 31. Collins PL, Hill MG, Camargo E, Grosfeld H, Chanock RM, Murphy BR. 1995. Production of infectious human respiratory syncytial virus from cloned cDNA confirms an essential role for the transcription elongation factor from the 5' proximal open reading frame of the M2 mRNA in gene expression and provides a capability for vaccine development. *Proc. Natl. Acad. Sci. U. S. A.* 92:11563–11567.
 32. Davidson W, Frego L, Peet GW, Kroe RR, Labadia ME, Lukas SM, Snow RJ, Jakes S, Grygon CA, Pargellis C, Werneburg BG. 2004. Discovery and characterization of a substrate selective p38 α inhibitor. *Biochemistry* 43:11658–11671.
 33. Hirsch V, Adger-Johnson D, Campbell B, Goldstein S, Brown C, Elkins WR, Montefiori DC. 1997. A molecularly cloned, pathogenic, neutralization-resistant simian immunodeficiency virus, SIVsmE543-3. *J. Virol.* 71:1608–1620.
 34. Pazdrak K, Olszewska-Pazdrak B, Liu T, Takizawa R, Brasier AR, Garofalo RP, Casola A. 2002. MAPK activation is involved in posttranscriptional regulation of RSV-induced RANTES gene expression. *Am. J. Physiol. Lung Cell. Mol. Physiol.* 283:L364–L372.
 35. Neininger A, Kontoyiannis D, Kotlyarov A, Winzen R, Eckert R, Volk HD, Holtmann H, Kollias G, Gaestel M. 2002. MK2 targets AU-rich elements and regulates biosynthesis of tumor necrosis factor and interleukin-6 independently at different post-transcriptional levels. *J. Biol. Chem.* 277:3065–3068.
 36. Stoecklin G, Stubbs T, Kedersha N, Wax S, Rigby WF, Blackwell TK, Anderson P. 2004. MK2-induced tristetraprolin:14-3-3 complexes prevent stress granule association and ARE-mRNA decay. *EMBO J.* 23:1313–1324.
 37. Santangelo PJ, Lifland AW, Curt P, Sasaki Y, Bassell GJ, Lindquist ME, Crowe JE, Jr. 2009. Single molecule-sensitive probes for imaging RNA in live cells. *Nat. Methods* 6:347–349.
 38. Lindquist ME, Mainou BA, Dermody TS, Crowe JE, Jr. 2011. Activation of protein kinase R is required for induction of stress granules by respiratory syncytial virus but dispensable for viral replication. *Virology* 413:103–110.
 39. Lifland AW, Jung J, Alonas E, Zurla C, Crowe JE, Jr, Santangelo PJ. 2012. Human respiratory syncytial virus nucleoprotein and inclusion bodies antagonize the innate immune response mediated by MDA5 and MAVS. *J. Virol.* 86:8245–8258.
 40. Love DC, Hanover JA. 2005. The hexosamine signaling pathway: deciphering the “O-GlcNAc code.” *Sci. STKE* 2005:re13.
 41. Golks A, Guerini D. 2008. The O-linked N-acetylglucosamine modification in cellular signalling and the immune system. ‘Protein modifications: beyond the usual suspects’ review series. *EMBO Rep.* 9:748–753.
 42. Shi Y, Gaestel M. 2002. In the cellular garden of forking paths: how p38 MAPKs signal for downstream assistance. *Biol. Chem.* 383:1519–1536.
 43. Dehennaut V, Slomianny MC, Page A, Vercoutter-Edouart AS, Jessus C, Michalski JC, Vilain JP, Bodart JF, Lefebvre T. 2008. Identification of structural and functional O-linked N-acetylglucosamine-bearing proteins in *Xenopus laevis* oocyte. *Mol. Cell. Proteomics* 7:2229–2245.
 44. Hanover JA, Krause MW, Love DC. 2010. The hexosamine signaling pathway: O-GlcNAc cycling in feast or famine. *Biochim. Biophys. Acta* 1800:80–95.
 45. Hart GW, Housley MP, Slawson C. 2007. Cycling of O-linked beta-N-acetylglucosamine on nucleocytoplasmic proteins. *Nature* 446:1017–1022.
 46. Pathak S, Borodkin VS, Albarbarawi O, Campbell DG, Ibrahim A, van Aalten DM. 2012. O-GlcNAcylation of TAB1 modulates TAK1-mediated cytokine release. *EMBO J.* 31:1394–1404.
 47. Collins PL, Hill MG, Cristina J, Grosfeld H. 1996. Transcription elongation factor of respiratory syncytial virus, a nonsegmented negative-strand RNA virus. *Proc. Natl. Acad. Sci. U. S. A.* 93:81–85.
 48. Cartee TL, Wertz GW. 2001. Respiratory syncytial virus M2-1 protein requires phosphorylation for efficient function and binds viral RNA during infection. *J. Virol.* 75:12188–12197.
 49. Hardy RW, Wertz GW. 2000. The Cys(3)-His(1) motif of the respiratory syncytial virus M2-1 protein is essential for protein function. *J. Virol.* 74:5880–5885.